

# Comparative Analysis of Solar-to-Fuel Conversion Efficiency: A Direct, One-Step Electrochemical CO<sub>2</sub> Reduction Reactor versus a Two-Step, Cascade Electrochemical CO<sub>2</sub> Reduction Reactor

Electrochemical and photoelectrochemical (PEC) CO<sub>2</sub> reduction (CO<sub>2</sub>R) have the potential to produce sustainable, zero greenhouse gas emission fuels and chemicals.<sup>1–6</sup> One of the key components in a PEC CO<sub>2</sub> reduction device is the electrocatalyst materials for the CO<sub>2</sub>R reaction. While significant research advances have been made in the development of CO<sub>2</sub> reduction catalysts and in the understanding of the reaction mechanisms, selective, active, and stable catalyst materials have yet to be identified to directly convert CO<sub>2</sub> into higher reduction products, such as ethanol and ethylene.<sup>3,7–9</sup> In contrast, several electrocatalyst systems have exhibited promising selectivity and activity for the first two-electron, two-proton process, such as CO<sub>2</sub>R to CO or formate.<sup>5,6,10,11</sup> For example, nanostructured silver electrodes,<sup>12–14</sup> metal dichalcogenides,<sup>15</sup> and single metal atoms in graphene nanosheets<sup>16,17</sup> exhibited high Faradaic efficiency (FE) and high reaction rates for CO<sub>2</sub>R to CO. A Pd/C nanoparticle-based catalyst incorporated in a 10% efficient solar-to-formate conversion device also exhibited near-unity FE at 10s of mA cm<sup>-2</sup> for CO<sub>2</sub>R to formate.<sup>5,6</sup> Hence, one alternative strategy is to leverage the efficient first two-electron, two-proton reaction by using a two-step, cascade CO<sub>2</sub> reactor, in which the first catalytic reactor converts CO<sub>2</sub> into CO or formate and the second catalytic reactor converts CO or formate into higher-order reduction products such as ethanol or ethylene. Herein, the solar-to-fuel (STF) conversion efficiencies in a direct, one-step CO<sub>2</sub> reduction reactor and a two-step, cascade CO<sub>2</sub> reduction reactor were analyzed and compared for two distinctive device configurations.

In the first discrete device configuration, as illustrated for a one-step reactor (Figure 1a) and a two-step reactor (Figure 1b), power matching between the power-generating component, the photovoltaic cell, and the fuel-forming component, the electrochemical cell, was achieved by using DC-to-DC converters. In the discrete configuration, the STF conversion efficiency,  $\eta_{\text{STF\_discrete}}$  is defined as the following<sup>18</sup>

$$\eta_{\text{STF\_discrete}} = \eta_{\text{PV}} \cdot \eta_{\text{ETF}} \cdot \eta_{\text{DC-DC converter}} \quad (1)$$

where  $\eta_{\text{PV}}$  is the solar-to-electric conversion efficiency of a photovoltaic cell,  $\eta_{\text{DC-DC converter}}$  is the efficiency of a DC-to-DC converter, and  $\eta_{\text{ETF}}$  is the electric-to-fuel conversion efficiency of the electrochemical cell. The  $\eta_{\text{PV}}$  was set to be 42.4% for a tandem junction cell at the Shockley–Queisser (S–Q) limit, and the  $\eta_{\text{DC-DC converter}}$  was set to be 85%.<sup>18</sup> The  $\eta_{\text{ETF\_one\_Step}}$  and  $\eta_{\text{ETF\_two\_Step}}$  were defined as the following for the electric-to-fuel conversion efficiencies of the one-step

reactor and the two step reactor, respectively. Note that while the first and the second reactors in the two-step reactor are connected in series, the  $\eta_{\text{ETF\_two\_Step}}$  is *not* simply the product of the electric-to-fuel conversion efficiency of the first reactor and the second reactor. The detailed derivation for the  $\eta_{\text{ETF}}$  can be found in [Supporting Information](#).

$$\eta_{\text{ETF\_one\_Step}} = \frac{E_{\text{CO}_2 \text{ to C}_2\text{H}_6\text{O}} \cdot \text{FE}_{\text{CO}_2 \text{ to C}_2\text{H}_6\text{O}}}{V_{\text{CO}_2 \text{ to C}_2\text{H}_6\text{O}}} \quad (2)$$

$$\eta_{\text{ETF\_two\_Step}} = \frac{\frac{3}{2} E_{\text{CO}_2 \text{ to C}_2\text{H}_6\text{O}} \cdot \text{FE}_{\text{CO to C}_2\text{H}_6\text{O}}}{\frac{\text{FE}_{\text{CO to C}_2\text{H}_6\text{O}}}{2 \text{FE}_{\text{CO}_2 \text{ to CO}}} V_{\text{CO}_2 \text{ to CO}} + V_{\text{CO to C}_2\text{H}_6\text{O}}} \quad (3)$$

where  $E_{\text{CO}_2 \text{ to C}_2\text{H}_6\text{O}}$  is the thermodynamic voltage window for the CO<sub>2</sub> reduction to C<sub>2</sub>H<sub>6</sub>O reaction,  $\text{FE}_{\text{CO}_2 \text{ to C}_2\text{H}_6\text{O}}$ ,  $\text{FE}_{\text{CO}_2 \text{ to CO}}$ , and  $\text{FE}_{\text{CO to C}_2\text{H}_6\text{O}}$  are the FEs for the CO<sub>2</sub> reduction to C<sub>2</sub>H<sub>6</sub>O, CO<sub>2</sub> reduction to CO, and CO reduction to C<sub>2</sub>H<sub>6</sub>O reactions, respectively,  $V_{\text{CO}_2 \text{ to C}_2\text{H}_6\text{O}}$ ,  $V_{\text{CO}_2 \text{ to CO}}$ , and  $V_{\text{CO to C}_2\text{H}_6\text{O}}$  are the total voltages required for the CO<sub>2</sub> reduction to C<sub>2</sub>H<sub>6</sub>O, CO<sub>2</sub> reduction to CO, and CO reduction to C<sub>2</sub>H<sub>6</sub>O reactions, respectively.

The total voltages,  $V_{\text{CO}_2 \text{ to C}_2\text{H}_6\text{O}}$ ,  $V_{\text{CO}_2 \text{ to CO}}$ , and  $V_{\text{CO to C}_2\text{H}_6\text{O}}$  were calculated as the following

$$V_{\text{CO}_2 \text{ to C}_2\text{H}_6\text{O}} = E_{\text{CO}_2 \text{ to C}_2\text{H}_6\text{O}} + V_{\text{anode\_loss}} + V_{\text{cathode\_loss\_CO}_2 \text{ to C}_2\text{H}_6\text{O}} + V_{\text{transport loss}} \quad (4)$$

$$V_{\text{CO}_2 \text{ to CO}} = E_{\text{CO}_2 \text{ to CO}} + V_{\text{anode\_loss}} + V_{\text{cathode\_loss\_CO}_2 \text{ to CO}} + V_{\text{transport loss}} \quad (5)$$

$$V_{\text{CO to C}_2\text{H}_6\text{O}} = E_{\text{CO to C}_2\text{H}_6\text{O}} + V_{\text{anode\_loss}} + V_{\text{cathode\_loss\_CO to C}_2\text{H}_6\text{O}} + V_{\text{transport loss}} \quad (6)$$

where  $E_{\text{CO}_2 \text{ to CO}}$  and  $E_{\text{CO to C}_2\text{H}_6\text{O}}$  are the thermodynamic voltage windows for the CO<sub>2</sub> reduction to CO and CO reduction to C<sub>2</sub>H<sub>6</sub>O reactions, respectively,  $V_{\text{anode\_loss}}$  is the

Received: June 26, 2018

Accepted: July 6, 2018

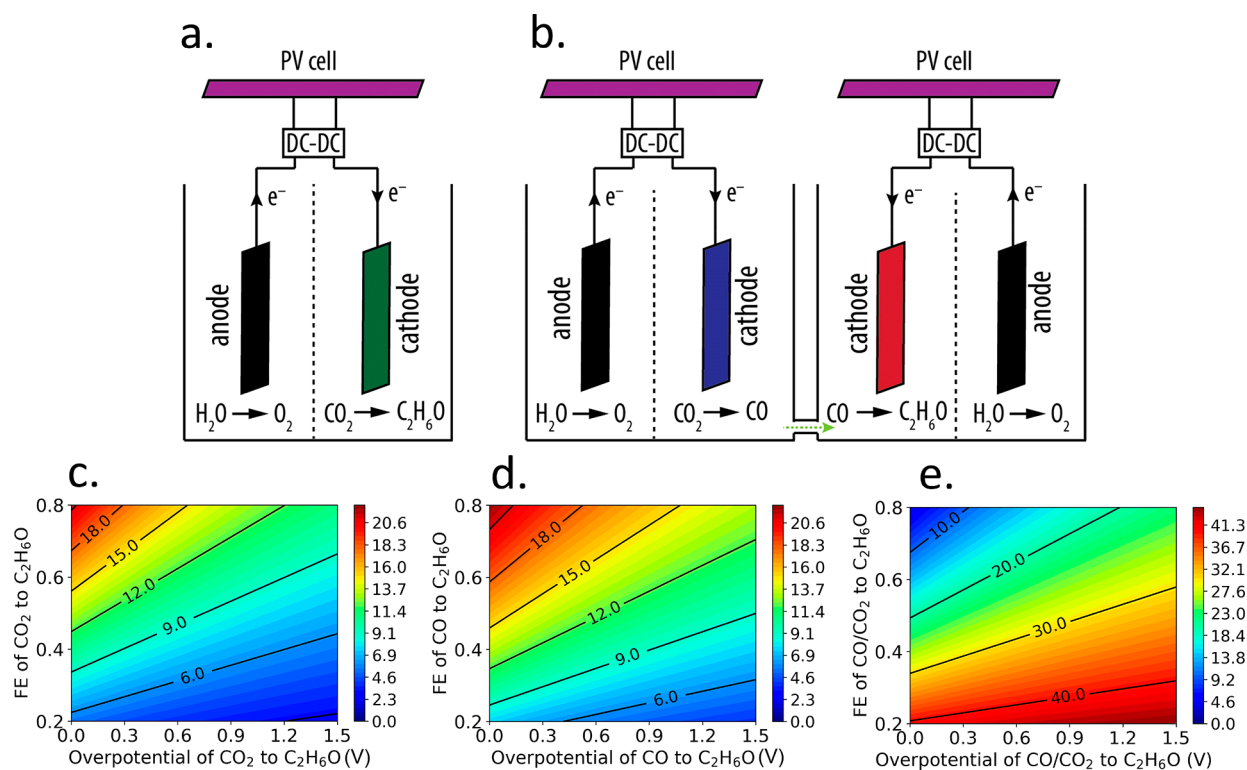


**Figure 1.** Scheme illustrations of the series-connected photovoltaic and electrochemical cells in a one-step reactor (a) and in a two-step reactor (b). STF conversion efficiency of the one-step reactor (c) and the two-step reactor (d) of  $CO_2$  reduction to  $C_2H_6O$  at different cathodic overpotentials and FE combinations. (e) Relative percentage increase of the STF conversion efficiency of the two-step  $CO_2$  reduction reactor cell relative to the one-step  $CO_2$  reduction reactor.

anodic voltage loss for water oxidation,  $V_{\text{cathode\_loss\_}CO_2 \text{ to } C_2H_6O}$ ,  $V_{\text{cathode\_loss\_}CO_2 \text{ to } CO}$ , and  $V_{\text{cathode\_loss\_}CO \text{ to } C_2H_6O}$  are the cathodic voltage losses for  $CO_2$  reduction to  $C_2H_6O$  or  $CO$  and  $CO$  reduction to  $C_2H_6O$ , respectively, and  $V_{\text{transport\_loss}}$  is the transport loss from the electrolyte and membrane separators in the device. In this analysis, the anodic overpotentials for the oxygen evolution reaction (OER), the transport losses in the cell, the overpotential and FE for  $CO_2$  reduction to  $CO$  in the two-step reactor, as well as the thermodynamic voltage windows for the reactions are given in Table 1. On the basis

**Table 1.** Reaction Voltage Window and Voltage Loss Assumptions in the Analysis

	one-step reactor	two-step reactor (mV)	
	(mV)	first reactor	second reactor
reaction window	1.14 V	1.33 V	1.05 V
anodic overpotential	300	300	300
cathodic overpotential	variable	100	variable
transport losses in the cell	100	100	100

of the demonstrated performances, the transport loss in the cell<sup>19,20</sup> and the anodic overpotential loss<sup>21,22</sup> in both reactors were assumed to be 100 and 300 mV, respectively. On the basis of the state-of-the-art catalyst performances,<sup>12–17,23,24</sup> the cathodic overpotential and FE for  $CO_2$  reduction to  $CO$  were assumed to be 100 mV and 90% for the first step reaction in the two-step reactor, respectively. The cathodic overpotential and FE for  $CO_2$  or  $CO$  reduction to ethanol were the two

parametric variables in the study. Figure 1c,d shows the  $\eta_{\text{STF\_discrete}}$  as a function of the FE and overpotential for  $CO_2$  or  $CO$  reduction into  $C_2H_6O$  for the one-step reactor and the two-step reactor, respectively. The  $\eta_{\text{STF}}$  values in both reactors were highly dependent on the FE and overpotentials for the fuel-forming reactions. In the discrete device configuration,  $\eta_{\text{STF}}$  values as high as 21.4 and 22.3% can be achieved in the one-step reactor and the two-step reactor, respectively. The electrochemical cell efficiencies,  $\eta_{\text{ETF\_one\_Step}}$  and  $\eta_{\text{ETF\_two\_Step}}$  as a function of the overpotential and FE for  $CO_2$  or  $CO$  reduction were also plotted in Figure S1. Because in the discrete device configuration the power-generating component and the fuel-forming component can be optimized independently,  $\eta_{\text{STF}}$  for more realistic PV cells with different  $\eta_{\text{PV}}$  values can be obtained readily (see Figure S2 for Si-based PV cells<sup>25</sup>). Figure 1e shows the relative percentage increase of the  $\eta_{\text{STF\_discrete}}$  of the two-step reactor compared to the one-step reactor. The  $\eta_{\text{STF\_discrete}}$  of the two-step reactor was higher than that of the one-step reactor at all reduction overpotential and FE combinations. In the high overpotential region in which the catalyst performed poorly, a relative percentage increase as high as 45% was observed between the two reactors. The low overpotential and high FE for  $CO_2$  reduction to  $CO$ , which have been demonstrated in experimental reports,<sup>12–17,23,24</sup> add the first two electrons and two protons onto  $CO_2$  very efficiently for the subsequent reaction and, hence, improve the overall conversion efficiency of the device in the two-step reactor.

The second device configuration contained wireless, integrated photoelectrodes for a one-step reactor (Figure 2a) and a two-step reactor (Figure 2b). The  $\eta_{\text{STF\_integrated\_one\_Step}}$  and  $\eta_{\text{STF\_integrated\_two\_Step}}$  values can be calculated as the

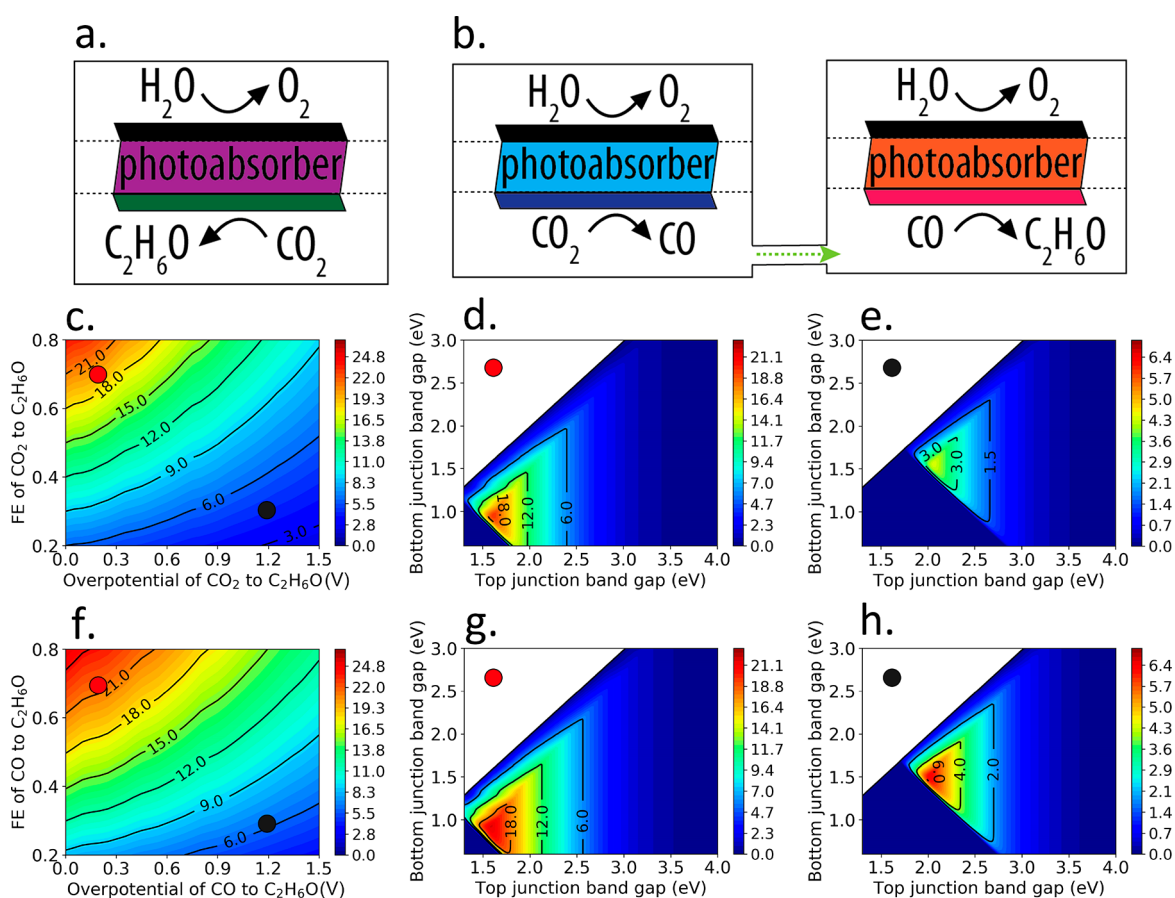


**Figure 2.** Schematic illustrations of the integrated photoelectrodes for PEC CO<sub>2</sub>R in a one-step reactor (a) and in a two-step reactor (b). STF conversion efficiency of the one-step reactor (c) and the two-step reactor (f) of CO<sub>2</sub> reduction to C<sub>2</sub>H<sub>6</sub>O at different cathodic overpotentials and FE combinations when the tandem photoabsorbers behave at the S–Q limit. STF conversion efficiency for different bottom and top junction band gap combinations of the one-step reactor with a cathodic overpotential of 0.2 V and a FE of 70% (d) and a cathodic overpotential of 1.2 V and a FE of 30% (e). STF conversion efficiency for different bottom and top junction band gap combinations of the two-step reactor with a cathodic overpotential of 0.2 V and a FE of 70% (g) and a cathodic overpotential of 1.2 V and a FE of 30% (h).

following, and a detailed derivation is included in the Supporting Information

$$\eta_{\text{STF\_integrated\_one\_Step}} = \frac{J_{\text{CO}_2 \text{ to C}_2\text{H}_6\text{O}} E_{\text{CO}_2 \text{ to C}_2\text{H}_6\text{O}} \text{FE}_{\text{CO}_2 \text{ to C}_2\text{H}_6\text{O}}}{P_{\text{in}}} \quad (7)$$

$$\eta_{\text{STF\_integrated\_two\_Step}} = \frac{3E_{\text{CO}_2 \text{ to C}_2\text{H}_6\text{O}} \text{FE}_{\text{CO to C}_2\text{H}_6\text{O}}}{P_{\text{in}} \left( \frac{1}{J_{\text{CO}_2 \text{ to CO}} \text{FE}_{\text{CO}_2 \text{ to CO}}} + \frac{2}{J_{\text{CO to C}_2\text{H}_6\text{O}} \text{FE}_{\text{CO to C}_2\text{H}_6\text{O}}} \right)} \quad (8)$$

where  $J_{\text{CO}_2 \text{ to C}_2\text{H}_6\text{O}}$ ,  $J_{\text{CO}_2 \text{ to CO}}$ , and  $J_{\text{CO to C}_2\text{H}_6\text{O}}$  are the operating current densities for CO<sub>2</sub> reduction to C<sub>2</sub>H<sub>6</sub>O, CO<sub>2</sub> reduction to CO, and CO reduction to C<sub>2</sub>H<sub>6</sub>O, respectively, and  $P_{\text{in}}$  is the incident illumination intensity. The incident illumination intensity was set to be 100 mW cm<sup>-2</sup>. The anodic overpotentials for OER, the transport losses in the cell, the overpotential and FE for CO<sub>2</sub> reduction to CO in the two-step reactor, as well as the thermodynamic voltage windows for the reactions were assumed to be the same as the discrete device configuration and are tabulated in Table 1. Figure 2c,f shows the optimal STF conversion efficiency,  $\eta_{\text{STF\_integrated}}$ , of the one-step reactor and the two-step reactor as a function of the reduction overpotentials and FEs in the integrated device

configuration. For each overpotential and FE combination, all of the permutations of the band gaps in the tandem photoabsorbers were calculated, and the optimal  $\eta_{\text{STF\_integrated}}$  (Figure 2c,f) was achieved by using the optimal band gap combinations in the tandem photoabsorbers. In the integrated device configuration and among all of the overpotential and FE combinations, the two-step reactor exhibited higher STF conversion efficiency than the one-step reactor (the relative percentage increase was plotted in Figure S3). At two typical overpotential and FE combinations, 0.2 V/70% and 1.2 V/30%, the  $\eta_{\text{STF\_integrated}}$  values as a function of the top junction band gap and bottom junction band gap were shown in Figure 2d,e,g,h. As the overpotential for the reduction reaction increased, the band gap values in the tandem photoabsorbers also increased to accommodate the increase of the total operating voltage in order to achieve the optimal  $\eta_{\text{STF\_integrated}}$ . Note that the optimal band gap combination for CO<sub>2</sub> reduction to CO in the two-step reactor was 1.7 eV/1.0 eV, which was very similar to the optimal band gap combinations for the solar-driven water-splitting cell<sup>26</sup> due to similar cathodic voltage losses in the two systems. The optimized top and bottom band gap values of the two-step reactor were slightly lower than those of the one-step reactor (Table S1), which was due to the lower voltage window for the CO reduction to C<sub>2</sub>H<sub>6</sub>O relative to the CO<sub>2</sub> reduction to C<sub>2</sub>H<sub>6</sub>O.

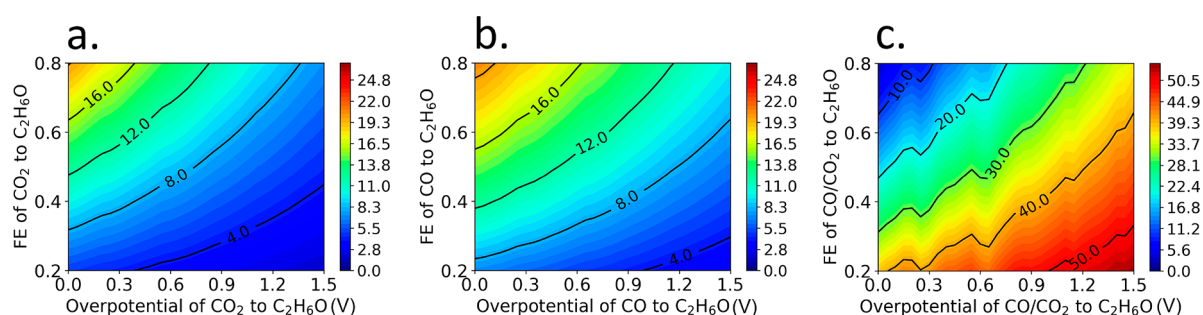


**Figure 3.** STF conversion efficiency of the one-step reactor (a) and the two-step reactor (b) of CO<sub>2</sub> reduction to C<sub>2</sub>H<sub>6</sub>O at different cathodic overpotentials and FE combinations with high-performing tandem junction photoabsorbers. (c) Relative percentage increase of STF conversion efficiency of the two-step CO<sub>2</sub> reduction reactor relative to the one-step CO<sub>2</sub> reduction reactor with high-performing tandem junction photoabsorbers.

The  $\eta_{\text{STF, integrated}}$  was also calculated using more realistic and high-performing photoabsorbers. Figure 3a,b shows  $\eta_{\text{STF, integrated}}$  of the one-step reactor and the two-step reactor as a function of the reduction overpotentials and FEs with high-performing tandem photoabsorbers. For high-performance semiconductors, we assume that 90% of incident photons above the band gap of the semiconductor were absorbed, and there is a semiconductor external radiative efficiency (ERE; see the Supporting Information for the definition of ERE) of 3%, meaning that the radiative recombination represents 3% of the total recombination. The optimal  $\eta_{\text{STF, integrated}}$  values for both reactors with high-performance light absorbers were  $\sim 20\%$  lower than photoabsorbers simulated at the S–Q limit due to light reflection and nonradiative recombination losses. Figure 3c shows the relative percentage increase of the optimal  $\eta_{\text{STF, integrated}}$  of the two-step reactor compared to that of the one-step reactor as a function of the reduction overpotentials and FEs. Similarly to the discrete system as shown in Figure 1e, the optimal  $\eta_{\text{STF, integrated}}$  of the two-step reactor was higher than that of the one-step reactor at all reduction overpotential and FE combinations. In some electrocatalytic performance regions, a relative percentage increase as high as 54% was observed between the two reactors. The first two-electron, two-proton reduction reaction from CO<sub>2</sub> to CO with a high FE and low overpotential significantly improved the overall optimal  $\eta_{\text{STF, integrated}}$ . In addition, the CO reduction to C<sub>2</sub>H<sub>6</sub>O reaction had a lower voltage window than the direct CO<sub>2</sub> reduction to C<sub>2</sub>H<sub>6</sub>O, which eased the requirement for large-band-gap light absorbers.

In addition to the higher overall STF conversion efficiency in the two-step reactor, different electrolytes, electrocatalysts, and membrane separators could be used and optimized individually in the two-step reactor at different reaction rates. For the direct, one-step reactor, the catholyte pH window is limited to near-neutral pH values due to the acid–base equilibrium of CO<sub>2</sub> in the solution.<sup>27,28</sup> The concentration of dissolved CO<sub>2</sub> at the electrode surface would quickly approach zero in high-pH electrolytes, which would significantly limit the partial current density for CO<sub>2</sub>R.<sup>29,30</sup> In contrast, the CO reduction in the two-step reactor does not have such constraints, and in fact, CO reduction often exhibited higher selectivity and higher reaction rates in high-pH electrolytes due to the suppression of the hydrogen evolution reaction (HER).<sup>2</sup> On the other hand, the two-step reactor also introduces additional engineering complexities relative to the one-step reactor. For instance, the CO produced from the first step needs to be purified and separated from other reduction

products, and the production rate of CO from the first reactor needs to be matched with the consumption rate of CO in the second reactor. From the technoeconomic point of view, the two-step reactor will likely to have a higher initial installation cost and capital expenditure (CapEx) than the one-step reactor. In the discrete device configuration in particular, the choice between the two-step reactor and the one-step reactor will likely be based on the cost of the renewable electricity and the CapEx differential of the electrolysis units.

In summary, the STF conversion efficiencies of a direct, one-step reactor that electrochemically reduces CO<sub>2</sub> to C<sub>2</sub>H<sub>6</sub>O and a two-step, cascade reactor that electrochemically reduces CO<sub>2</sub> to CO followed by a subsequent electrochemical reduction of CO to C<sub>2</sub>H<sub>6</sub>O were evaluated and compared quantitatively. By leveraging the efficient and selective first two-electron, two-proton process from CO<sub>2</sub> to CO, the optimal STF conversion efficiency of the two-step reactor was higher than that of the one-step reactor at all cathodic overpotential and FE combinations. The analysis shows that in some electrocatalyst performance regions with high cathodic overpotentials a relative improvement in STF conversion efficiency as high as 54% can be obtained by using the two-step reactor. The alternative, two-step CO<sub>2</sub> reactor design can provide new pathways to efficient and selective CO<sub>2</sub> reduction to higher reduction products.

Xinghao Zhou<sup>†,‡,§</sup>

Chengxiang Xiang<sup>\*,†,§</sup>

<sup>†</sup>Joint Center for Artificial Photosynthesis, California Institute of Technology, Pasadena, California 91125, United States

<sup>‡</sup>Department of Applied Physics and Materials Science, Division of Engineering and Applied Science, California Institute of Technology, Pasadena, California 91125, United States

<sup>§</sup>Division of Chemistry and Chemical Engineering, California Institute of Technology, Pasadena, California 91125, United States

## ■ ASSOCIATED CONTENT

### Supporting Information

The Supporting Information is available free of charge on the ACS Publications website at DOI: 10.1021/acseenergylett.8b01077.

Detailed derivations for the electric-to-fuel conversion efficiency and solar-to-fuel conversion efficiency in the two-step reactors, definition of high-performing light-

absorber materials, optimal band gap combinations in the integrated solar-fuel devices, and supplementary figures for electric-to-fuel conversion efficiencies for both reactors (PDF)

## AUTHOR INFORMATION

### ORCID

Xinghao Zhou: 0000-0001-9229-7670

Chengxiang Xiang: 0000-0002-1698-6754

### Notes

Views expressed in this Viewpoint are those of the authors and not necessarily the views of the ACS.

The authors declare no competing financial interest.

## ACKNOWLEDGMENTS

This material is based upon work performed by the Joint Center for Artificial Photosynthesis, a DOE Energy Innovation Hub, supported through the Office of Science of the U.S. Department of Energy under Award Number DE-SC0004993.

## REFERENCES

- (1) Gattrell, M.; Gupta, N.; Co, A. A Review of the Aqueous Electrochemical Reduction of CO<sub>2</sub> to Hydrocarbons at Copper. *J. Electroanal. Chem.* **2006**, *594*, 1–19.
- (2) Han, L.; Zhou, W.; Xiang, C. High-Rate Electrochemical Reduction of Carbon Monoxide to Ethylene Using Cu-Nanoparticle-Based Gas Diffusion Electrodes. *ACS Energy Lett.* **2018**, *3*, 855–860.
- (3) Torelli, D. A.; Francis, S. A.; Crompton, J. C.; Javier, A.; Thompson, J. R.; Brunschwig, B. S.; Soriaga, M. P.; Lewis, N. S. Nickel–Gallium-Catalyzed Electrochemical Reduction of CO<sub>2</sub> to Highly Reduced Products at Low Overpotentials. *ACS Catal.* **2016**, *6*, 2100–2104.
- (4) Li, K.; Peng, B.; Peng, T. Recent Advances in Heterogeneous Photocatalytic CO<sub>2</sub> Conversion to Solar Fuels. *ACS Catal.* **2016**, *6*, 7485–7527.
- (5) Min, X.; Kanan, M. W. Pd-catalyzed Electrohydrogenation of Carbon Dioxide to Formate: High Mass Activity at Low Overpotential and Identification of the Deactivation Pathway. *J. Am. Chem. Soc.* **2015**, *137*, 4701–4708.
- (6) Zhou, X.; Liu, R.; Sun, K.; Chen, Y.; Verlage, E.; Francis, S. A.; Lewis, N. S.; Xiang, C. Solar-driven Reduction of 1 atm of CO<sub>2</sub> to Formate at 10% Energy-conversion Efficiency by Use of a TiO<sub>2</sub>-protected III–V Tandem Photoanode in Conjunction with a Bipolar Membrane and a Pd/C Cathode. *ACS Energy Lett.* **2016**, *1*, 764–770.
- (7) Cook, R. L.; MacDuff, R. C.; Sammells, A. F. High Rate Gas Phase CO<sub>2</sub> Reduction to Ethylene and Methane Using Gas Diffusion Electrodes. *J. Electrochem. Soc.* **1990**, *137*, 607–608.
- (8) Ren, D.; Deng, Y.; Handoko, A. D.; Chen, C. S.; Malkhandi, S.; Yeo, B. S. Selective Electrochemical Reduction of Carbon Dioxide to Ethylene and Ethanol on Copper (I) Oxide Catalysts. *ACS Catal.* **2015**, *5*, 2814–2821.
- (9) Dinh, C.-T.; Burdyny, T.; Kibria, M. G.; Seifitokaldani, A.; Gabardo, C. M.; García de Arquer, F. P.; Kiani, A.; Edwards, J. P.; De Luna, P.; Bushuyev, O. S.; et al. CO<sub>2</sub> Electroreduction to Ethylene via Hydroxide-mediated Copper Catalysis at an Abrupt Interface. *Science* **2018**, *360*, 783–787.
- (10) Rosen, B. A.; Salehi-Khojin, A.; Thorson, M. R.; Zhu, W.; Whipple, D. T.; Kenis, P. J.; Masel, R. I. Ionic Liquid-mediated Selective Conversion of CO<sub>2</sub> to CO at Low Overpotentials. *Science* **2011**, *334*, 643–644.
- (11) Sheng, W.; Kattel, S.; Yao, S.; Yan, B.; Liang, Z.; Hawxhurst, C. J.; Wu, Q.; Chen, J. G. Electrochemical Reduction of CO<sub>2</sub> to Synthesis Gas with Controlled CO/H<sub>2</sub> Ratios. *Energy Environ. Sci.* **2017**, *10*, 1180–1185.
- (12) Guo, S.-X.; Li, F.; Chen, L.; MacFarlane, D. R.; Zhang, J. Polyoxometalate-Promoted Electrochemical CO<sub>2</sub> Reduction at Nanostructured Silver in Dimethylformamide. *ACS Appl. Mater. Interfaces* **2018**, *10*, 12690–12697.
- (13) Ma, M.; et al. Selective and Efficient Reduction of Carbon Dioxide to Carbon Monoxide on Oxide-Derived Nanostructured Silver Electrocatalysts. *Angew. Chem.* **2016**, *128*, 9900–9904.
- (14) Rosen, J.; Hutchings, G. S.; Lu, Q.; Rivera, S.; Zhou, Y.; Vlachos, D. G.; Jiao, F. Mechanistic Insights into the Electrochemical Reduction of CO<sub>2</sub> to CO on Nanostructured Ag Surfaces. *ACS Catal.* **2015**, *5*, 4293–4299.
- (15) Asadi, M.; Kim, K.; Liu, C.; Addepalli, A. V.; Abbasi, P.; Yasaei, P.; Phillips, P.; Behranginia, A.; Cerrato, J. M.; Haasch, R.; et al. Nanostructured Transition Metal Dichalcogenide Electrocatalysts for CO<sub>2</sub> Reduction in Ionic Liquid. *Science* **2016**, *353*, 467–470.
- (16) Jiang, K.; Siahrostami, S.; Akey, A. J.; Li, Y.; Lu, Z.; Lattimer, J.; Hu, Y.; Stokes, C.; Gangisetty, M.; Chen, G.; et al. Transition-Metal Single Atoms in a Graphene Shell as Active Centers for Highly Efficient Artificial Photosynthesis. *Chem.* **2017**, *3*, 950–960.
- (17) Jiang, K.; Siahrostami, S.; Zheng, T.; Hu, Y.; Hwang, S.; Stavitski, E.; Peng, Y.; Dynes, J.; Gangisetty, M.; Su, D.; et al. Isolated Ni Single Atoms in Graphene Nanosheets for High-performance CO<sub>2</sub> Reduction. *Energy Environ. Sci.* **2018**, *11*, 893–903.
- (18) Chen, Y.; Xiang, C.; Hu, S.; Lewis, N. S. Modeling the Performance of an Integrated Photoelectrolysis System with 10 × Solar Concentrators. *J. Electrochem. Soc.* **2014**, *161*, F1101–F1110.
- (19) Hernandez-Pagan, E. A.; Vargas-Barbosa, N. M.; Wang, T.; Zhao, Y.; Smotkin, E. S.; Mallouk, T. E. Resistance and Polarization Losses in Aqueous Buffer-Membrane Electrolytes for Water-splitting Photoelectrochemical Cells. *Energy Environ. Sci.* **2012**, *5*, 7582–7589.
- (20) Jin, J.; Walczak, K.; Singh, M. R.; Karp, C.; Lewis, N. S.; Xiang, C. X. An Experimental and Modeling/Simulation-Based Evaluation of the Efficiency and Operational Performance Characteristics of an Integrated, Membrane-Free, Neutral pH Solar-Driven Water-Splitting System. *Energy Environ. Sci.* **2014**, *7*, 3371–3380.
- (21) McCrory, C. C. L.; Jung, S.; Ferrer, I. M.; Chatman, S. M.; Peters, J. C.; Jaramillo, T. F. Benchmarking Hydrogen Evolving Reaction and Oxygen Evolving Reaction Electrocatalysts for Solar Water Splitting Devices. *J. Am. Chem. Soc.* **2015**, *137*, 4347.
- (22) Zhang, B.; Zheng, X. L.; Voznyy, O.; Comin, R.; Bajdich, M.; Garcia-Melchor, M.; Han, L. L.; Xu, J. X.; Liu, M.; Zheng, L. R.; et al. Homogeneously Dispersed Multimetal Oxygen-Evolving Catalysts. *Science* **2016**, *352*, 333–337.
- (23) Jovanov, Z. P.; Hansen, H. A.; Varela, A. S.; Malacrida, P.; Peterson, A. A.; Nørskov, J. K.; Stephens, I. E. L.; Chorkendorff, I. Opportunities and Challenges in the Electrocatalysis of CO<sub>2</sub> and CO Reduction using Bifunctional Surfaces: A Theoretical and Experimental Study of Au–Cd Alloys. *J. Catal.* **2016**, *343*, 215–231.
- (24) Kauffman, D. R.; Alfonso, D.; Matranga, C.; Qian, H.; Jin, R. Experimental and Computational Investigation of Au<sub>25</sub> Clusters and CO<sub>2</sub>: A Unique Interaction and Enhanced Electrocatalytic Activity. *J. Am. Chem. Soc.* **2012**, *134*, 10237–10243.
- (25) Green, M. A.; Emery, K.; Hishikawa, Y.; Warta, W.; Dunlop, E. D.; Levi, D. H.; Ho-Baillie, A. W. Y. Solar Cell Efficiency Tables (Version 49). *Prog. Photovoltaics* **2017**, *25*, 3–13.
- (26) Xiang, C.; Weber, A. Z.; Ardo, S.; Berger, A.; Chen, Y. K.; Coridan, R.; Fountaine, K. T.; Haussener, S.; Hu, S.; Liu, R.; et al. Modeling, Simulation, and Implementation of Solar-Driven Water-Splitting Devices. *Angew. Chem., Int. Ed.* **2016**, *55*, 12974–12988.
- (27) Kumar, B.; Llorente, M.; Froehlich, J.; Dang, T.; Sathrum, A.; Kubiak, C. P. Photochemical and Photoelectrochemical Reduction of CO<sub>2</sub>. *Annu. Rev. Phys. Chem.* **2012**, *63*, 541–569.
- (28) Hori, Y.; Wakebe, H.; Tsukamoto, T.; Koga, O. Electrocatalytic Process of CO Selectivity in Electrochemical Reduction of CO<sub>2</sub> at Metal Electrodes in Aqueous Media. *Electrochim. Acta* **1994**, *39*, 1833–1839.
- (29) Chen, Y.; Lewis, N. S.; Xiang, C. Modeling and Simulation of the Spatial and Light-Intensity Dependence of Product Distributions in an Integrated Photoelectrochemical CO<sub>2</sub> Reduction System. *ACS Energy Lett.* **2016**, *1*, 273–280.

(30) Hashiba, H.; Weng, L.-C.; Chen, Y.; Sato, H. K.; Yotsubashi, S.; Xiang, C.; Weber, A. Z. Effects of Electrolyte Buffer Capacity on Surface Reactant Species and the Reaction Rate of CO<sub>2</sub> in Electrochemical CO<sub>2</sub> Reduction. *J. Phys. Chem. C* **2018**, *122*, 3719–3726.